Heralding pure single photons: A comparison between counterpropagating and copropagating twin photons

Alessandra Gatti[1,2,*] and Enrico Brambilla[2]

[1]*Istituto di Fotonica e Nanotecnologie del CNR, Piazza Leonardo Da Vinci 32, Milano, Italy*

[2]*Dipartimento di Scienza e Alta Tecnologia dell' Università dell'Insubria, Via Valleggio 11, Como, Italy*

(Received 21 June 2017; revised manuscript received 28 November 2017; published 24 January 2018)

We investigate different strategies suitable to generate pure heralded single photons through spontaneous parametric down-conversion, comparing the counterpropagating geometry with more conventional copropagating configurations which enhance the purity of the heralded photon state through the technique of group-velocity matching. We derive general results for the Schmidt number associated to the temporal modes, which provide a quantitative estimate of the purity. An analysis of the correlation of twin photons in the temporal domain provides a more physical view of the mechanisms that permit to eliminate the temporal entanglement of the state and to generate high-purity heralded photons. The efficiency of the various strategies and the individual properties of the heralded photons thereby generated are then compared.

DOI: 10.1103/PhysRevA.97.013838

I. INTRODUCTION

Single-photon states are of outstanding interest in modern quantum optics, as the basis of fundamental tests of quantum mechanics and of a variety of quantum technologies (see, e.g., [1,2] for recent surveys of single-photon techniques and applications). In order to generate truly single photons, one of the most efficient methods is based on a conditional measurement, where a two-photon state is generated and the presence of a single photon is *heralded* by detection of its partner. To this end, parametric processes such as spontaneous parametric down-conversion (PDC) or four-wave mixing (FWM), where one or two photons belonging to a high-energy pump laser are occasionally converted into pairs of photons, are routinely employed. The conservation laws ruling these microscopic processes originate a quantum correlation in the spatial and temporal degrees of freedom of the pair, which typically extends over broad spectral and angular bandwidths. Such a high-dimensional entanglement may represent a resource for broadband quantum technologies, but is detrimental for the purity of heralded single photons because detection of the trigger photon projects the state of its twin in a highly mixed state. This represents a limitation for quantum communication and information protocols where single photons are required to be indistinguishable and capable of high-visibility interference.

The recent development of wave-guided PDC (see [3] and references therein) and of FWM in single-mode fibers [4] opened the possibility to control the spatial degrees of freedom, and to generate the twin photons into a single or few spatial modes. In order to eliminate also the spectrotemporal correlation, a possibility is filtering hard enough that a single spectral mode is selected, but then the efficiency of the source is reduced. In order to achieve pure heralded photons with high fluxes, considerable effort has been devoted to find alternative techniques, which directly reduce the degree of entanglement of the source in order to produce uncorrelated twin photons [5–13]. In such a way, a conditional measurement projects the field in a pure single-photon state rather than in a mixed state. In the standard copropagating geometry [Fig. 1(b)], this task requires careful techniques of group-velocity matching, which can be implemented only in some materials and tuning conditions [5,8].

In recent years, the counterpropagating configuration of PDC, where twin photons are emitted along opposite directions [Fig. 1(a)], emerged as a promising source of heralded pure single photons without the need of group-velocity matching [14,15]. Proposed by Harris in the 1960's [16] and implemented in 2007 by Canalias *et al.* [17], this configuration presents the challenge of requiring a very short poling of the nonlinear material [18,19]. On the other hand, counterpropagating twin photons and twin beams possess peculiar and attractive features, such as their narrow-band character [14,20–22] and the potential to generate in the high-gain regime a robust continuous-variable entanglement [23,24]. In the spontaneous regime, twin photons may be naturally generated in either spectrally entangled or decorrelated states by simply modifying the pump pulse duration (or crystal length), without the need of special tuning conditions [14]. Similar features have recently been described in counterpropagating FWM [25].

In this work we focus on the PDC process, and on the temporal correlation of twin photons thereby generated, making a parallel analysis of the two copropagating and counterpropagating geometries (Fig. 1) as sources of heralded single photons. By a systematic comparison of the two configurations, we aim at providing an understanding of the physical mechanisms under which temporal correlation emerges and can eventually be eliminated, which may turn useful to optimize the existing configurations and to design new ones. Even though our analysis is restricted to the PDC process, some of our results may qualitatively hold also for FWM.

*Alessandra.Gatti@mi.infn.it

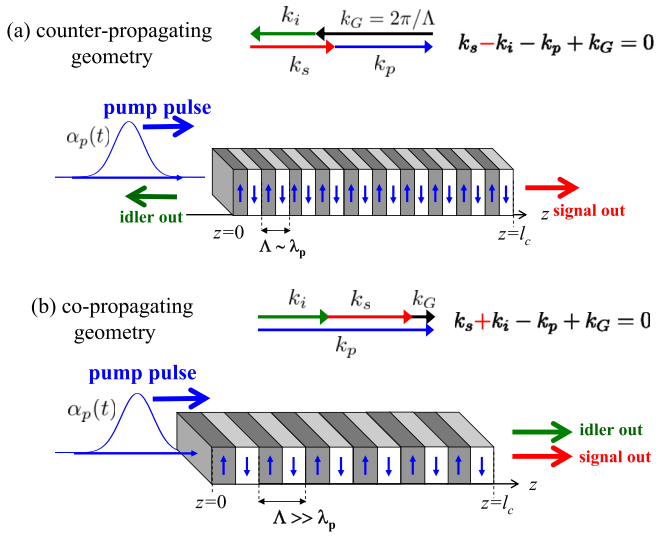

FIG. 1. (a) Scheme of twin-photon generation in the (a) counterpropagating and (b) copropagating geometries. In the case (a) quasi-phase matching at first order requires submicrometer poling periods $\Lambda \sim \lambda_p$ of the nonlinear material.

Our analysis is partially based on the correlation of twin photons in the temporal domain. Apart from pioneering studies [26], this approach is not standard in the literature [5–13,15], which mostly focused on their spectral correlation, and provides, in our opinion, a more direct physical view. In particular, it will show that the temporal correlation between twin photons can be eliminated only creating conditions such that the timing provided by the pump pulse is more precise than that offered by detecting any of the twin photons. In addition, this approach is probably the only useful one in the counterpropagating geometry, where measurements are more likely to be resolved in time than in frequency, because of the narrow spectral bandwidth. From a quantitative point of view, we will derive an approximated formula for the Schmidt number, to our knowledge not present in the former literature, which holds for both geometries and gives a simple means for evaluating the degree of purity of the heralded photon based only on two parameters of the source. Finally, the individual spectrotemporal properties of the heralded photons, which are of great importance in view of different applications, will be investigated in parallel. In particular, we will see that either narrow-band or broadband pure heralded photons are characteristic of the two geometries, and that different strategies of group-velocity matching lead to very different efficiencies of pair production.

The paper is organized as follows: After introducing in Sec. II the two geometries, Sec. III studies the Schmidt number, while Sec. IV describes the temporal correlation of twin photons, in terms both of general analytic results and of numerical calculations. Finally, Sec. V describes the spectrotemporal properties of heralded photons and compares the efficiency of heralding of the different strategies investigated.

II. COUNTERPROPAGATING AND COPROPAGATING GEOMETRIES

As in most of the previous literature, our analysis is restricted to the temporal domain, assuming either a single-mode wave-guided configuration, or that a small angular bandwidth is collected.

In the counterpropagating geometry shown in Fig. 1(a), a coherent pump pulse of central frequency ω_p and temporal profile $\alpha_p(t)$ impinges a $\chi^{(2)}$ crystal of length l_c from the left face, and generates counterpropagating photon pairs with, say, the idler photon back-propagating towards the laser source. This process requires periodically poled structures with short poling periods Λ, such that the momentum associated to the nonlinear grating of the nonlinearity $k_G = \frac{2\pi m}{\Lambda}$, $m = \pm 1, \pm 3 \ldots$, can approximately compensate the momentum of the pump photon. The central frequencies of the down-converted fields ω_s and $\omega_i = \omega_p - \omega_s$ are thus determined by the quasi-phase-matching condition

$$k_s - k_i = k_p - k_G, \tag{1}$$

where $k_j = \frac{\omega_j}{c} n_j(\omega_j)$, $j = s,i,p$, are the wave numbers at the central frequencies ω_j.

In the copropagating geometry [Fig. 1(b)] all the three fields propagate along the positive z direction. In this case, quasi-phase matching requires

$$k_s + k_i = k_p - k_G, \tag{2}$$

where the case $k_G = 0$ corresponds to ordinary phase matching.

The efficiency of down-conversion is described by a dimensionless gain parameter g, proportional to the peak amplitude of the pump laser, the crystal length, and the nonlinear susceptibility. Considering the spontaneous regime $g \ll 1$, the signal-idler state at the crystal output can be written as a power series expansion in g (see, e.g., [14] for details). Retaining terms up to first order in g, it takes the well-known form

$$|\phi\rangle = |0\rangle + |\phi_2\rangle, \tag{3}$$

$$|\phi_2\rangle = \int d\Omega_s d\Omega_i \psi(\Omega_s,\Omega_i) \hat{a}_s^\dagger(\Omega_s) \hat{a}_i^\dagger(\Omega_i)|0\rangle, \tag{4}$$

corresponding to the superposition of the vacuum and the two-photon state $|\phi_2\rangle$. Here, $\hat{a}_s^\dagger(\Omega_s)$ and $\hat{a}_i^\dagger(\Omega_i)$ are signal and idler photon creation operators in the frequency domain, Ω_j being the offset from the reference frequency ω_j, and

$$\psi(\Omega_s,\Omega_i) = \frac{g}{\sqrt{2\pi}} \tilde{\alpha}_p(\Omega_s + \Omega_i) \mathrm{sinc}\left[\frac{\mathcal{D}^{\pm}(\Omega_s,\Omega_i) l_c}{2}\right] e^{i\beta(\Omega_s,\Omega_i)} \tag{5}$$

is the spectral biphoton amplitude, which gives the joint probability amplitude of detecting a signal photon at frequency $\omega_s + \Omega_s$ and an idler photon at frequency $\omega_i + \Omega_i$. In formula (5), $\tilde{\alpha}_p(\Omega) = \int \frac{dt}{\sqrt{2\pi}} e^{i\Omega t} \alpha_p(t)$ is the pump spectral amplitude, where the temporal profile $\alpha_p(t)$ is normalized to its peak value; $\mathcal{D}^{\pm}(\Omega_s,\Omega_i) l_c$ is the phase-mismatch function, where here and in the following the indices $+$ and $-$ refer to the counterpropagating and copropagating geometries in Figs. 1(a) and 1(b), respectively:

$$\mathcal{D}^{\pm}(\Omega_s,\Omega_i) = \begin{cases} k_p(\Omega_s + \Omega_i) - k_s(\Omega_s) + k_i(\Omega_i) + k_G, \\ k_p(\Omega_s + \Omega_i) - k_s(\Omega_s) - k_i(\Omega_i) + k_G. \end{cases} \tag{6}$$

Finally,

$$\beta(\Omega_s,\Omega_i) = \frac{l_c}{2}[k_s(\Omega_s) + k_i(\Omega_i) + k_p(\Omega_s + \Omega_i)] \quad (7)$$

is a global phase, acquired during the propagation along the crystal in the absence of any nonlinear effect by a pair of photons generated at the crystal center $z = l_c/2$. As described in [14,22–24], the different sign in front of the idler wave number in Eq. (6) is at the origin of the radically different properties of PDC in the two geometries. This is best seen by expanding the phase mismatch (6) at first order around the reference frequencies (corresponding to $\Omega_j = 0$)

$$\mathcal{D}^{\pm}(\Omega_s,\Omega_i)\frac{l_c}{2} \approx \frac{l_c}{2}[(k'_p \pm k'_i)\Omega_i + (k'_p - k'_s)\Omega_s] \equiv \tau_i^{\pm}\Omega_i + \tau_s\Omega_s, \quad (8)$$

where $k'_j \equiv v_{gj}^{-1} = (\frac{dk_j}{d\Omega_j})_{\Omega_j=0}$ is the inverse group velocity of wave j and the characteristic times

$$\tau_s = \frac{1}{2}\left(\frac{l_c}{v_{gp}} - \frac{l_c}{v_{gs}}\right), \quad (9)$$

$$\tau_i^{\pm} = \frac{1}{2}\left(\frac{l_c}{v_{gp}} \pm \frac{l_c}{v_{gi}}\right) \quad (10)$$

involve either the difference or the sum of the group velocities of the pump and the down-converted wave, depending whether they copropagate or counterpropagate. These constants represent the characteristic temporal separations between the pump and the down-converted wave packets, precisely the delays between the exit time of the pump $t_{Ap} = \frac{l_c}{v_{gp}}$ and those of two twin photons generated at the crystal center. In the copropagating case τ_s and τ_i^- are determined by the group-velocity mismatch (GVM) with respect to the pump, and are typically on the same order of magnitude, unless some particular strategy of group-velocity matching is employed. In contrast, in the counterpropagating case, the time constant associated to the backward photon τ_i^+ involves the group-velocity sum (GVS) and is on the order of the photon transit time across the crystal, which largely exceeds the GVM time.

An analogous linear approximation of the global phase in Eq. (7) gives

$$\beta(\Omega_s,\Omega_i) \approx \text{const} + t_{As}\Omega_s + t_{Ai}\Omega_i, \quad (11)$$

where

$$t_{Aj} = \frac{l_c}{2v_{gj}} + \frac{l_c}{2v_{gp}} = t_{Ap} - \tau_j^- \qquad (j = s,i) \quad (12)$$

are the exit times of the centers of the signal and idler wave packets, and can be considered as the times at which two twin photons down-converted from the pump peak at $z = l_c/2$, pictured as wave packets propagating without deformation, arrive at the end faces of the crystal.

Finally, we notice that the linear approximation in Eqs. (8) and (11) amounts to neglecting the temporal dispersion: this is well justified in the counterpropagating configuration, which involves narrow down-conversion spectra [14,17,22], but it is less justified in the copropagating case because of the larger bandwidths in play. In particular, it ceases to be valid in the absence of a GVM between twin photons $\tau_s \simeq \tau_i^-$ (e.g., for type-I PDC close to degeneracy), a condition that, as we shall see, is not relevant to our discussion because it prevents from generating pure heralded photons.

III. ENTANGLEMENT QUANTIFICATION

The degree of entanglement of the state is here characterized by the Schmidt number [27,28], which also estimates the number of independent modes participating to the entangled state [29]. It is defined as the inverse of the purity of the state of each separate subsystem

$$\mathcal{K} = \frac{1}{\text{Tr}\{\hat{\rho}_s^2\}} = \frac{1}{\text{Tr}\{\hat{\rho}_i^2\}}, \quad (13)$$

where $\hat{\rho}_s$, $\hat{\rho}_i$ are the reduced density matrix of the signal and idler when the PDC state (3) is conditioned to a photon count. For example, for the signal $\hat{\rho}_s = \frac{1}{\langle\phi_2|\phi_2\rangle}\text{Tr}_i\{|\phi_2\rangle\langle\phi_2|\}$. The inverse of the Schmidt number thus straightforwardly gives the degree of purity of the heralded photon state, via a single parameter that can be calculated without resorting to the explicit Schmidt decomposition.

In this work, the Schmidt number $\mathcal{K}$ is calculated in two ways:

(i) "Exact" results are obtained by numerical calculation of the integral formula [30]

$$\mathcal{K} = \frac{\mathcal{N}^2}{B}, \quad (14)$$

$$\mathcal{N} = \int d\Omega_s \int d\Omega_i\, |\psi(\Omega_s,\Omega_i)|^2, \quad (15)$$

$$B = \int d\Omega_s \ldots \int d\Omega'_i [\psi(\Omega_s,\Omega_i)\psi(\Omega'_s,\Omega'_i) \times \psi^*(\Omega_s,\Omega'_i)\psi^*(\Omega'_s,\Omega_i)] \quad (16)$$

valid for any biphoton state of the form (4). The biphoton amplitude ψ appearing under the integrals is calculated by using the complete Sellmeier dispersion formula in [31–33].

(ii) Approximated analytical results are derived within the "Gaussian approximation" of the spectral amplitude extensively used in former studies of copropagating PDC [5,6]. This consists in replacing the sinc function in Eq. (5) by a Gaussian of its argument, and then using the linear approximations (8) and (11), obtaining thereby

$$\text{sinc}\frac{\mathcal{D}^{\pm}(\Omega_s,\Omega_i)l_c}{2} \to e^{-\gamma\left[\frac{\mathcal{D}^{\pm}(\Omega_s,\Omega_i)l_c}{2}\right]^2} \approx e^{-\gamma(\tau_s\Omega_s+\tau_i^{\pm}\Omega_i)^2}, \quad (17)$$

where, e.g., $\gamma = \frac{1}{6}$ if one equates the leading order of the Taylor expansions of the sinc and the Gaussian, or $\gamma = 0.193$ if one requires that they have the same full width at half maximum. In addition, one has to consider a Gaussian pump pulse $\alpha_p(t) = e^{-t^2/2T_p^2}$, of duration T_p and spectral width $\Delta\Omega_p = 1/T_p$, so that $\tilde{\alpha}_p(\Omega) = T_p e^{-\frac{T_p^2}{2}\Omega_p^2}$. The spectral amplitude (5) takes then the Gaussian form

$$\psi(\Omega_s,\Omega_i) \to \frac{gT_p}{\sqrt{2\pi}} e^{i[t_{As}\Omega_s + t_{Ai}\Omega_i]} e^{-\sum_{i,j=s,i} c_{ij}\Omega_i\Omega_j}, \quad (18)$$

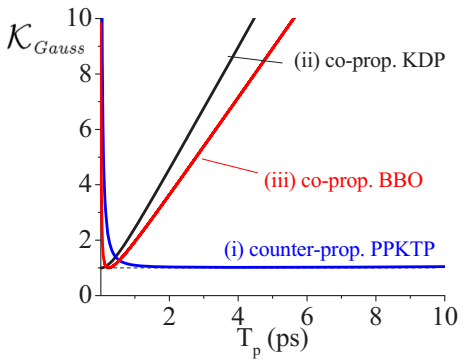

FIG. 2. Schmidt number $\mathcal{K}$ in the Gaussian approximation [Eq. (22)], as a function of the pump duration for (i) counterpropagating PPKTP, (ii) copropagating KDP $\eta = 0$, (iii) copropagating BBO $\eta = -1$ (parameters in Table I). In case (i) separability is achieved in a much broader range of pump durations and for longer pulses.

where constant phase terms have been omitted and the real coefficients c_{ij} (see also [6]) are

$$c_{ss} = \frac{T_p^2}{2} + \gamma {\tau_s}^2, \tag{19}$$

$$c_{ii} = \frac{T_p^2}{2} + \gamma {\tau_i^{\pm}}^2, \tag{20}$$

$$c_{is} = \frac{T_p^2}{2} + \gamma \tau_s \tau_i^{\pm}. \tag{21}$$

The approximation (18) allows to extract analytical results, providing a straightforward comparison between the two cases. Inserting Eq. (18) inside Eqs. (15) and (16), and performing the Gaussian integrals involved, we find a single formula that holds for any PDC configuration:

$$\mathcal{K}_{\rm Gauss} = \sqrt{\frac{c_{ss}c_{ii}}{c_{ss}c_{ii} - c_{si}^2}} = \left[1 + \left(1 + \frac{2\gamma\,\tau_s\tau_i^{\pm}}{T_p^2}\right)^2 \frac{T_p^2}{2\gamma|\tau_i^{\pm} - \tau_s|^2}\right]^{1/2}. \tag{22}$$

This result gives a simple way of estimating the degree of purity $1/\mathcal{K}$ of heralded single photons for any crystal length and dispersion relation in the medium. We notice that in this formula the various parameters that characterize the PDC process (crystal length, dispersion relations for the three waves) have been condensed in only two parameters, i.e., in the two time constants τ_s and $\tau_i^{\pm}$ that rule the relative propagation of the three waves in a crystal of length l_c.

The Gaussian result (22), seen as a function of the pump duration T_p, presents for long-pump pulses a linear asymptote (Fig. 2):

$$\mathcal{K}_{\rm Gauss} \to \frac{T_p}{\sqrt{2\gamma}|\tau_i^{\pm} - \tau_s|} \qquad \text{for } T_p \gg \sqrt{2\gamma|\tau_i^{\pm}\tau_s|}. \tag{23}$$

corresponding to an entangled state with $\mathcal{K} \gg 1$;

by shortening the pump it reaches a minimum, and then it stays close to the curve

$$\mathcal{K}_{\rm Gauss} \to \frac{\sqrt{2\gamma}|\tau_s\tau_i^{\pm}|}{T_p|\tau_i^{\pm} - \tau_s|} \qquad \text{for } T_p \ll \sqrt{2\gamma|\tau_i^{\pm}\tau_s|}. \tag{24}$$

$\mathcal{K}_{\rm Gauss}$ takes its minimum (the purity takes its maximum) for

$$T_p^{\rm min} = \sqrt{2\gamma|\tau_s\tau_i^{\pm}|} \tag{25}$$

which is basically the geometrical mean between the two time constants $|\tau_s|$ and $|\tau_i^{\pm}|$. The minimum value of $\mathcal{K}$ is

$$\mathcal{K}_{\rm Gauss}^{\rm min} = \begin{cases} 1 & \text{for } \tau_s\tau_i^{\pm} \leqslant 0 \to \eta \leqslant 0, \\ \frac{\tau_i^{\pm}+\tau_s}{\tau_i^{\pm}-\tau_s} = \frac{1+\eta}{1-\eta} & \text{for } \tau_s\tau_i^{\pm} > 0 \to \eta > 0, \end{cases} \tag{26}$$

where for convenience of notation we introduced the parameter

$$\eta = \frac{\tau_s}{\tau_i^{\pm}}, \tag{27}$$

which can be positive or negative, and without loss of generality, we choose the signal and idler such that $|\tau_s| \leqslant |\tau_i^-|$ in the copropagating case. Thus,

$$-1 \leqslant \eta \leqslant 1. \tag{28}$$

As well known, the Gaussian approximation (18) predicts complete separability $\mathcal{K} = 1$ for $\eta \leqslant 0$, as can be immediately recognized by inspection of the mixed term c_{is} in Eq. (21). For $\eta = 0$, the ideal value $\mathcal{K} = 1$ is reached only asymptotically for $T_p \to 0$, while for $\eta < 0$ a separable state can be in principle obtained for a finite pump duration $T_p = T_p^{\rm min}$. Alternatively, for positive η, the two-photon state can be made almost separable by choosing a configuration for which η is sufficiently small because

$$\mathcal{K}_{\rm Gauss}^{\rm min} = \frac{1+\eta}{1-\eta} \simeq 1 + 2\eta \qquad \text{for } 0 < \eta \ll 1. \tag{29}$$

Remarkably, this last condition is naturally fulfilled in the counterpropagating case, where $|\eta| = \frac{|k_p' - k_s'|}{k_p' + k_i'} = \frac{|\tau_s|}{\tau_i^+} \ll 1$ for any choice of material and phase-matching conditions.

Figures 2 and 3 plot the Schmidt number $\mathcal{K}$ as a function of the pump duration, for three examples chosen as representatives of the two geometries (see Table I for parameters, and Appendix B for details), namely, (i) a generic counterpropagating configuration, not specifically optimized for separability, where $\eta \simeq 0.01$, and two copropagating configurations optimized for separability, with (ii) $\eta = 0$ and (iii) $\eta = -1$. Condition (ii) is referred to as *asymmetric group-velocity matching* and requires that the signal photon propagates with the same group velocity as the pump ($\tau_s = 0$) [6,7]. Condition (iii) corresponds to the *symmetric group-velocity matching*, and can be realized only in the copropagating case, requiring $\tau_s = -\tau_i^+$ [5,6]. They are usually difficult to satisfy in the visible range, but can be achieved in some $\chi^{(2)}$ material in the near infrared and at telecom wavelengths [2,5–8]. Experimental evidence of frequency decorrelated photon pairs through this technique was first reported in [7].

Figure 2 superimposes the three Schmidt numbers in the Gaussian approximation (22), while Fig. 3 (notice here the horizontal logarithmic scale) shows, for each example, a comparison between the Gaussian result and the exact one,

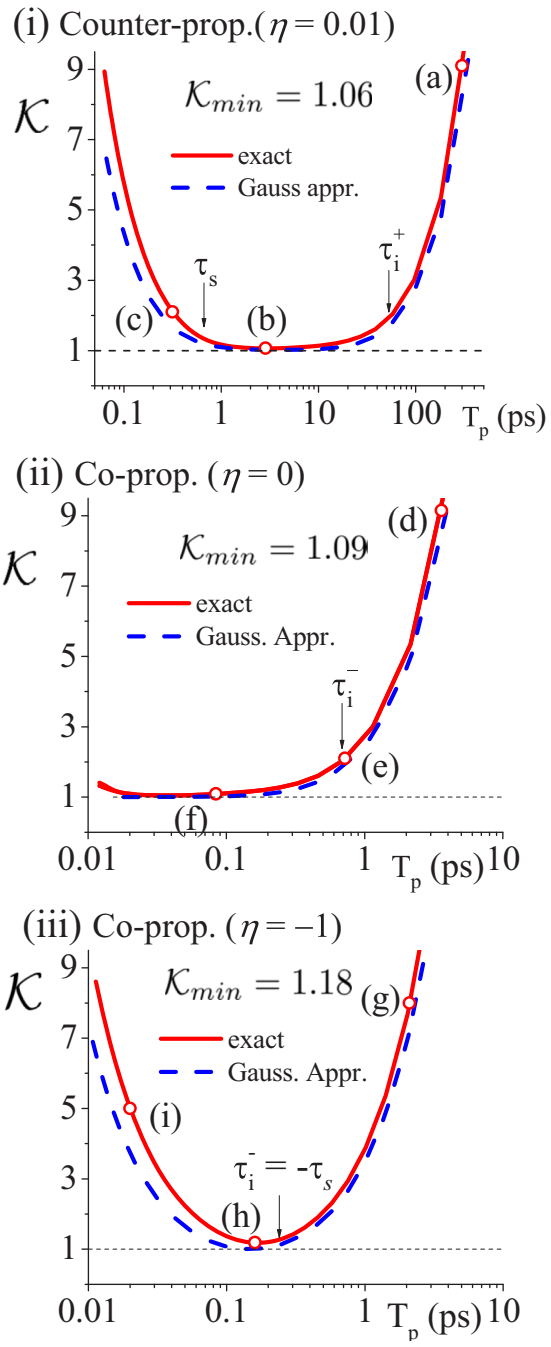

FIG. 3. Schmidt number $\mathcal{K}$: comparison of the Gaussian result (dashed blue lines) and the exact one (solid red lines) (i) counterpropagating PPKTP, (ii) copropagating KDP, (iii) copropagating BBO (parameters in Table I). In (i) the state is nearly separable for T_p intermediate between $\tau_s = 0.67$ ps and $\tau_i^+ = 63$ ps. In (ii) and (iii), separability is achieved only for subpicosecond pulses with $T_p \ll \tau_i^-$. The inverse of $\mathcal{K}_{\min}$ is the achievable degree of purity. The hollow red dots correspond to the plots in Figs. 4 and 5.

obtained by numerical integration of Eqs. (14)–(16). The Schmidt number curves show the same qualitative behavior in the three cases: for long-pump pulses the state is entangled, by shortening the pump pulse $\mathcal{K}$ reaches a minimum close to the ideal value $\mathcal{K}^{\min} = 1$, and then it grows again in the two examples with $\eta \neq 0$, while it stays close to the minimum in the example (ii) with $\eta = 0$. However, evident from these figures are the different ranges of pump durations T_p in which separability is achieved: the counterpropagating case displays a broad plateau with $\mathcal{K} \simeq 1$ for T_p in the range 2–10 ps, while in the copropagating case separability requires subpicosecond pulses, of duration $T_p \lesssim 100$ fs $\ll \tau_i^- = 720$ fs in case (ii), and $T_p \simeq T_p^{\min} = 147$ fs in case (iii).

Figure 3 also shows some discrepancy between the Gaussian results and the exact ones, especially for short-pump pulses. In particular, the minimum of $\mathcal{K}$ is always slightly larger than the Gaussian result (26), and never reaches the ideal value $\mathcal{K} = 1$ even for $\eta \leqslant 0$. Clearly, these discrepancies have to be ascribed both to the replacement of the sinc by a Gaussian and to the effect of dispersion, which becomes relevant only for short-pump pulses and/or long crystal. Because of this, the degree of purity achievable in the counterpropagating configuration with $\eta = 0.01$ is comparable to that obtained in the two cases with $\eta \leqslant 0$, which require much shorter pump pulses and stringent phase-matching conditions.

IV. TIME-DOMAIN VIEW: THE TEMPORAL CORRELATION OF TWIN PHOTONS

An alternative and perhaps more intuitive view of the problem is offered by the joint amplitude in the temporal domain, which is obtained by back Fourier transforming the joint spectral amplitude

$$\phi(t_s,t_i) = \int \frac{d\Omega_s}{\sqrt{2\pi}} \int \frac{d\Omega_i}{\sqrt{2\pi}} e^{-i(\Omega_s t_s + \Omega_i t_i)} \psi(\Omega_s,\Omega_i). \quad (30)$$

In terms of this function, the two-photon state (4) becomes

$$|\phi_2\rangle = \int dt_s dt_i \phi(t_s,t_i) \hat{a}_s^\dagger(t_s) \hat{a}_i^\dagger(t_i) |0\rangle, \quad (31)$$

where $\hat{a}_s^\dagger(t_s)$, $\hat{a}_i^\dagger(t_i)$ are photon creation operators in the time domain, and for example $\hat{a}_s^\dagger(t_s)|0\rangle \equiv |t_s\rangle$ represents the state with exactly one signal photon at time t_s at the crystal output face. Thus, $\phi(t_s,t_i)$, which was extensively analyzed in [14] in the counterpropagating case, represents the joint probability amplitude that a signal and an idler photon exit the crystal slab at times t_s and t_i, respectively, and describes the temporal correlation between the twin photons. The rate of coincidence counts at the crystal exit faces is then given by

$$G_{si}^{(2)}(t_s,t_i) \equiv \langle \hat{a}_s^\dagger(t_s) \hat{a}_s(t_s) \hat{a}_i^\dagger(t_i) \hat{a}_i(t_i) \rangle \approx |\phi(t_s,t_i)|^2. \quad (32)$$

Several plots of this correlation function are shown in Fig. 4, where the three columns correspond to the three examples in Table I. These plots were calculated from Eq. (30) without resorting to any approximation, by using the complete Sellmeier dispersion formula in [31–33]. If the linear approximations (8) and (11) are instead employed, the Fourier transform (30) can be explicitly calculated [14], obtaining

$$\phi(\bar{t}_s,\bar{t}_i) = \frac{g}{2|\tau_i^\pm - \tau_s|} \alpha_p\left(\frac{\bar{t}_s - \eta \bar{t}_i}{1-\eta}\right) \mathrm{Rect}\left(\frac{\bar{t}_s - \bar{t}_i}{|\tau_i^\pm - \tau_s|}\right), \quad (33)$$

TABLE I. Phase-matching conditions and characteristic time constants for the three crystals taken as examples: (i) periodically poled potassium titanyl phosphate (PPKTP), with 800 nm poling period for the counterpropagating configuration, (ii) potassium dihydrogen phosphate (KDP), and (iii) beta-barium triborate (BBO) crystals for the two copropagating configurations (Appendix B for details). τ_s, $\tau_i^{\pm}$, $T_p^{\min}$ are defined in Eqs. (9), (10), and (25), respectively.

Crystal	l_c (mm)	Phase matching (θ_p)	λ_p (nm)	λ_s (nm)	λ_i (nm)	τ_s (ps)	$\tau_i^{\pm}$ (ps)	$T_p^{\min}$ (ps)	η
(i) PPKTP	10	Type 0 e-ee (90°)	821.4	1141	2932	0.67	63	4.05	0.01
(ii) KDP	10	Type II e-oe (67.8°)	415	830	830	0	0.72	0	0
(iii) BBO	10	Type II e-oe (28.8°)	757	1514	1514	−0.237	0.237	0.147	−1

where constant phase factors have been omitted. The barred arguments

$$\bar{t}_j = t_j - t_{Aj}, \qquad j = s,i \tag{34}$$

are the exit times of the twin photons measured relative to the central exit times t_{Aj} of their wave packets, defined in Eq. (12); $\alpha_p(t)$ is the the pump temporal profile, and

$$\mathrm{Rect}\left(\frac{t}{\Delta\tau}\right) = \begin{cases} 1 & \text{for } t\epsilon\,[-\Delta\tau,\Delta\tau], \\ 0 & \text{elsewhere} \end{cases} \tag{35}$$

is the box function of width $2\Delta\tau$ and unitary height, where

$$\Delta\tau := |\tau_i^{\pm} - \tau_s| = \frac{l_c}{2}\left|\frac{1}{v_{gs}} \pm \frac{1}{v_{gi}}\right| \tag{36}$$

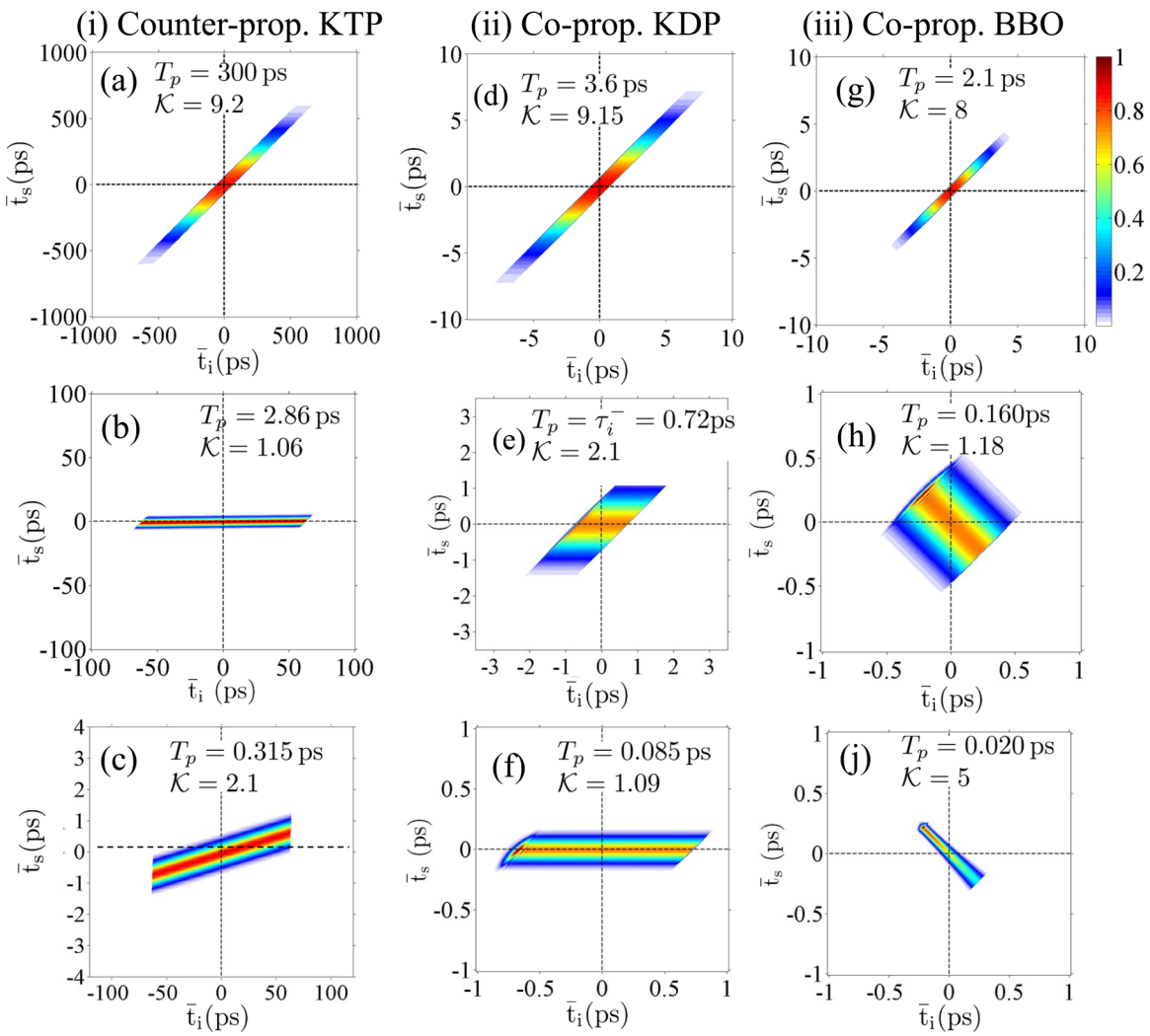

FIG. 4. Temporal correlation $|\phi(\bar{t}_s,\bar{t}_i)|^2$, representing the joint probability of finding a signal and an idler photon at times $t_s = \bar{t}_s + t_{\mathrm{As}}$ and $t_i = \bar{t}_i + t_{Ai}$ at the crystal exit faces, where the reference times t_{Aj} are defined in Eq. (12). In each column, the pump duration T_p decreases from top to bottom, in correspondence of the hollow red dots in Fig. 3. The plots identified by sublabels (a), (b), (f) correspond to the minima of $\mathcal{K}$ in Fig. 3, and represent the most separable conditions for each example.

represents the typical delay occurring between the exit times of two twin photons.

The result in Eq. (33) generalizes the expression found in [14] for the counterpropagating case to a generic geometry of PDC. Notice that it relies on linearizing the propagation phases, and in the copropagating case fails to be valid for $\tau_s \to \tau_i^-$.

Some of the mathematical findings in [14] apply then to both configurations. In particular, in the *limit of a long-pump pulse* $\boldsymbol{T_p \gg |\tau_i^\pm| \geqslant |\tau_s|}$,

$$\phi(\bar{t}_s,\bar{t}_i) \underset{T_p \gg |\tau_i^\pm|}{\longrightarrow} \frac{g}{2|\tau_i^\pm - \tau_s|}\alpha_p(\bar{t}_s)\mathrm{Rect}\left(\frac{\bar{t}_s - \bar{t}_i}{|\tau_i^\pm - \tau_s|}\right), \quad (37)$$

and the correlation exhibits a a sharp maximum along the diagonal $\bar{t}_s = \bar{t}_i$, of width $\Delta\tau$ (see the three upper plots in Fig. 4). In this limit, the joint temporal amplitude is not factorable in its arguments, and the two-photon state (31) is entangled. As detailed in Appendix A, the twin photons appear temporally correlated because they can be generated at any time along the long-pump pulse, but they are always generated together and the exit time of one photon can be predicted from that of its twin as $\bar{t}_s = \bar{t}_i$ within the narrower spread of their delays $\Delta\tau$. Accordingly, the number of entangled modes in this regime is $\mathcal{K} \propto \frac{T_p}{\Delta\tau}$, as predicted by the Gaussian formula in Eq. (23). Notice that the box shape of the correlation function in Eq. (37) is typical of the long-pump regime, where no information on the point where PDC occurred is available, so that the correlation reflects the flat distribution of the mutual time delays of the twins.

In the opposite *limit of an ultrashort-pump pulse* $\boldsymbol{T_p \ll |\tau_s| \leqslant |\tau_i^\pm|}$,

$$\phi(\bar{t}_s,\bar{t}_i) \underset{T_p \ll |\tau_s|}{\longrightarrow} \frac{g}{2|\tau_i^\pm - \tau_s|}\alpha_p\left(\frac{\bar{t}_s - \eta\bar{t}_i}{1-\eta}\right)\mathrm{Rect}\left[\frac{\bar{t}_s}{\tau_s}\right], \quad (38)$$

and the correlation function has a peak along the line $\bar{t}_s = \eta\bar{t}_i$, of width $\sim(1-\eta)T_p$, as approximately shown by Figs. 4(c) and 4(j). Thus, for $\eta \neq 0$, in this ultrashort-pump limit the state is again entangled: temporal correlation arises in this case not from the simultaneity of the twins, but from the information on the point where PDC occurred, which is now available, because both photons separate from the localized pump pulse during propagation. As explained in Appendix A, this knowledge permits to predict the arrival time of the signal from that of the idler as $\bar{t}_s = \eta\bar{t}_i$, within an uncertainty $\sim T_p(1-\eta)$. This is much smaller than the uncertainty $\sim|\tau_s|$ in the arrival time of the signal when the idler is not detected. Accordingly, the number of entangled modes is $\mathcal{K} \propto \frac{|\tau_s|}{T_p(1-\eta)}$ as predicted by Eq. (24). Notice the opposite signs of η in Figs. 4(c) and 4(j), reflecting the fact that the exit times of the twins relative to the pump are correlated for $\eta > 0$, while they are *anticorrelated* for $\eta < 0$ because in the latter case one photon is slower than the pump while the other is faster. For example, for $\eta = -1$, the correlation is peaked at $\bar{t}_s = -\bar{t}_i$, which for the original time arguments means $(t_s - t_{Ap}) = -(t_i - t_{Ap})$.

As discussed more in detail Appendix A, eliminating the correlation between twin photons requires that the timing gained by detecting the other member of the pair is not better than that offered by not detecting it, i.e., by only relying on the timing offered by the pump pulse. In this way, detection of one photon does not give any better information on the exit time of its twin than by not detecting it, and the two-photon state appears uncorrelated. This clearly requires a localized pump pulse and can be achieved in two ways:

(i) One photon (say the signal) propagates locked under the pump pulse but the other separates from it after some short propagation length. In these conditions, the pump provides a timing of the signal with a precision $\sim T_p$ similar as by detecting the idler. Mathematically, it corresponds to the intermediate pump limit $\boldsymbol{|\tau_i^\pm| \gg T_p \gg |\tau_s|}$, in which (as already shown in [14])

$$\phi(\bar{t}_s,\bar{t}_i) \underset{|\tau_i^\pm| \gg T_p \gg |\tau_s|}{\longrightarrow} \frac{g}{2|\tau_i^\pm - \tau_s|}\alpha_p(\bar{t}_s)\mathrm{Rect}\left(\frac{\bar{t}_i}{|\tau_i^\pm - \tau_s|}\right). \quad (39)$$

The biphoton correlation becomes separable in its arguments, as approximately shown by Figs. 4(b) and 4(f), implying that the two-photon state (31) is separable. This limit naturally arises in the counterpropagating case, where the two scales are separated, but needs not to exist in the copropagating case, where it basically requires that one of the two time constant vanishes, $\tau_s \to 0$.

(ii) Twin photons become displaced far enough away in time during propagation, still remaining close to the pump pulse. This can be achieved when one photon is faster than the pump while the other is slower, and for a pump duration $T_p \simeq |\tau_s|,|\tau_i^-|$, as in the symmetric group-velocity matching of the example (iii). In these conditions, twin photons are more simultaneous with the pump than between themselves, so that again the timing provided by the pump is better than that offered by the other twin (Appendix A). Notice that the purity of the heralded photons generated in this way [Fig. 4(h)] is somehow lower than in the other cases, and rather far from the ideal result $\mathcal{K}_{\min} = 1$ predicted by the Gaussian approximation. Such imperfect separability is a consequence of the sharp boundaries of the nonlinear medium, at the origin of the rectangular box function in Eq. (33) and of the sinc function in Eq. (5). The crystal boundaries have less impact on the separability when $|\eta| \ll 1$ because of the elongated shape of the temporal correlation [Figs. 4(b) and 4(f)]. These effects might be eliminated and the purity of the heralded photons increased by engineering a Gaussian nonlinearity profile of a poled crystal, as demonstrated by Branczyk *et al.* [12].

Remarkably, even though the temporal correlation $\phi(t_s,t_i)$ changes completely its shape in different pump regimes, when considered only as a function of the time difference $t_i - t_s$, it always retains a box-function shape. This means that if the coincidence count rate (32) at the crystal exit faces is registered only as a function of the delay between the twins, no information is gained about the entanglement or separability of the state. Indeed, if we rewrite the temporal correlation in Eq. (33) as a function of $\delta t = t_i - t_s$, we have

$$\phi(t_s,t_s+\delta t) \propto \alpha_p\left(\bar{t}_s - \frac{\eta}{1-\eta}\delta\bar{t}\right)\mathrm{Rect}\left(\frac{\delta\bar{t}}{\Delta\tau}\right),$$
$$\phi(t_i-\delta t,t_i) \propto \alpha_p\left(\bar{t}_i + \frac{1}{1-\eta}\delta\bar{t}\right)\mathrm{Rect}\left(\frac{\delta\bar{t}}{\Delta\tau}\right).$$

Then, if coincidence counts are measured only as a function of the delay δt, without detecting the absolute arrival time of

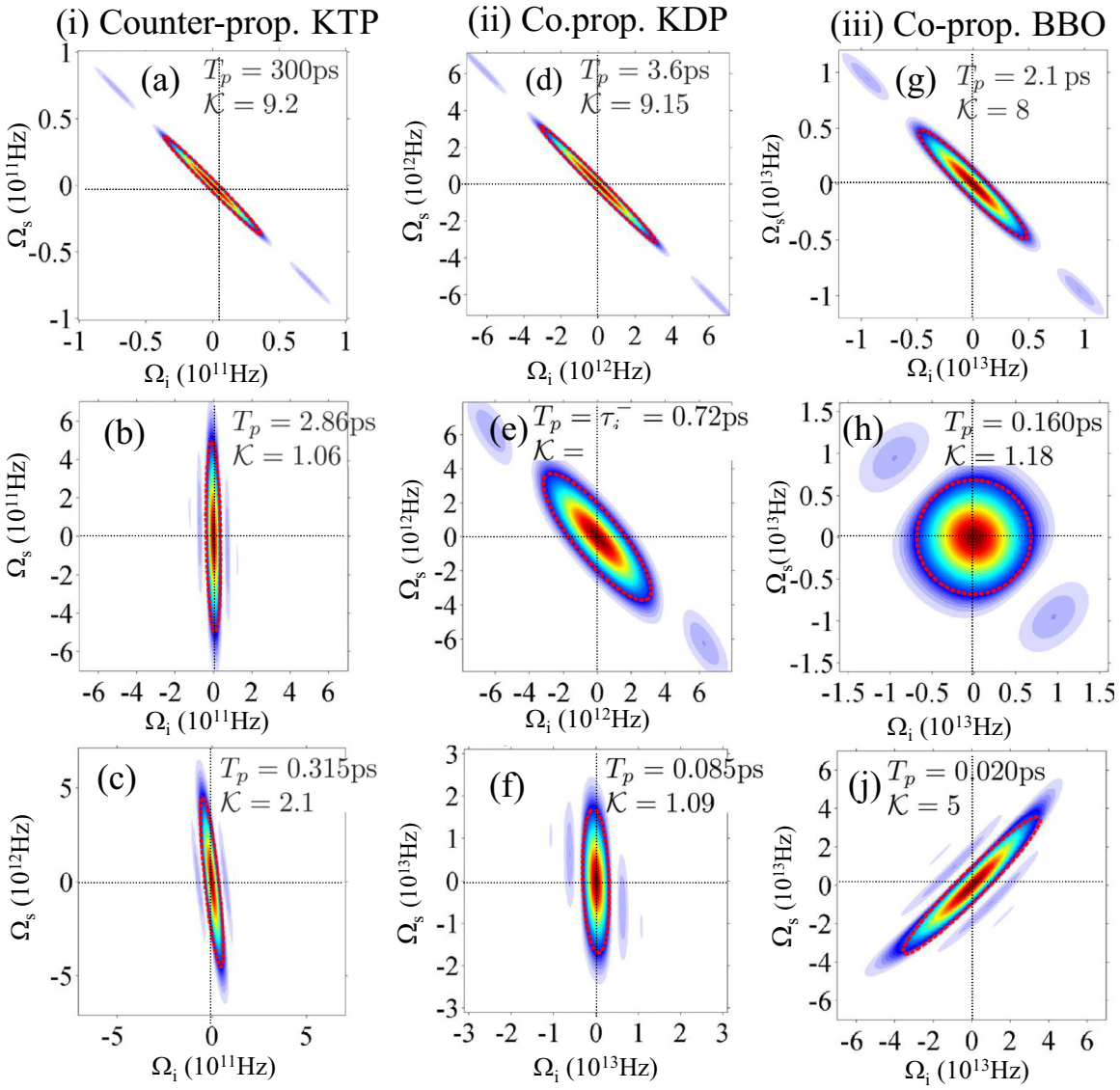

FIG. 5. Joint spectral probability $|\psi(\Omega_s,\Omega_i)|^2$ plotted for pump pulse durations decreasing from top to bottom, for the same parameters of Fig. 4 and in correspondence of the hollow red dots in Fig. 3. (b), (f), (h) Represent nearly separable situations. The red ellipses are the isoprobability curves of the Gaussian formula (18). Notice that in (c) the idler scale Ω_i is zoomed by a factor 10 with respect to the signal scale.

the signal or of the idler,

$$\bar{G}^{(2)}_{si}(\delta t) = \int dt_s |\phi(t_s, t_s+\delta t)|^2 = \int dt_i |\phi(t_i-\delta t, t_i)|^2 = \frac{\mathcal{N}}{2\Delta\tau}\mathrm{Rect}\left(\frac{\delta\bar{t}}{\Delta\tau}\right), \tag{40}$$

where $\mathcal{N} = g^2\frac{\sqrt{\pi}T_p}{2\Delta\tau}$ is the total number of photon pairs (see Sec. V). Therefore, the coincidence counts as a function of $t_i - t_s$ always reproduce the flat distribution of time delays characteristic of the spontaneous process, regardless whether the state is temporally entangled or separable.

It is also interesting to see how the results above described reflect in the shape of the joint spectral probability $|\psi(\Omega_i,\Omega_s)|^2$, plotted in Fig. 5 for the same parameters as in Fig. 4. The red ellipses here represent the curves $c_{11}\Omega_s^2 + c_{22}\Omega_i^2 + 2c_{12}\Omega_s\Omega_i = 1$ where according to the Gaussian formula (18) $|\psi|^2$ reduces by $1/e^2$, and permit to estimate visually the validity of the Gaussian approximation. The spectral correlation in this figure gives the complementary view with respect to the temporal correlation in Fig. 4, but obviously displays the same amount of entanglement: For long-pump pulses (top raw) the state is highly entangled in all the three examples, with the biphoton amplitude peaked along the diagonal $\Omega_s = -\Omega_i$ where energy conservation takes place. For short enough pump pulses [Figs. 5(c) and 5(i)] the state is again entangled, with the biphoton amplitude peaked along the line $\Omega_s = -\eta\Omega_i$ where momentum conservation, i.e., phase matching, is realized. Figures 5(b), 5(f), and 5(h) correspond to the optimal conditions for separability, and we see that in these cases the biphoton probability is a nearly factorable function of its arguments, being approximately an ellipse with its principal axes aligned along Ω_s and Ω_i. Notice, however, that in the example (iii) of symmetric group-velocity matching, the corresponding joint temporal probability in Fig. 4(h) exhibits a diamondlike shape, which gives much less a

geometrical evidence of separability, and indeed $\mathcal{K}_{\min} = 1.18$ is slightly higher than in the other two cases. In contrast, the biphoton probability in the spectral domain in Fig. 5(h) has a nearly circular shape, and deviations from factorability are only indicated by the side lobes of the sinc functions. This confirms the usefulness of taking the two complementary views in the temporal and spectral domains.

V. SPECTROTEMPORAL PROPERTIES OF HERALDED PHOTONS

Once assessed the conditions under which pure single heralded photons can be obtained, it is clearly important to study their individual properties in view of their use in quantum communication and metrology protocols (coupling with atoms, interferometry, etc.).

For spontaneous PDC, the marginal statistics of individual photons is described by their first-order coherence functions. In the temporal domain, for example, these functions are

$$\begin{aligned} G_s^{(1)}(t_s,t_s') &= \langle \hat{a}_s^\dagger(t_s)\hat{a}_s(t_s')\rangle \\ &= \int dt_i \phi^*(t_s,t_i)\phi(t_s',t_i), \end{aligned} \tag{41}$$

$$\begin{aligned} G_i^{(1)}(t_i,t_i') &= \langle \hat{a}_i^\dagger(t_i)\hat{a}_i(t_i')\rangle \\ &= \int dt_s \phi^*(t_s,t_i)\phi(t_s,t_i') \end{aligned} \tag{42}$$

with analogous definitions in the spectral domain. In terms of its temporal $G^{(1)}$, the reduced state of the heralded photon takes the form

$$\begin{aligned} \hat{\rho}_j &= \frac{1}{\mathcal{N}} \int dt \int dt' G_j^{(1)}(t',t)\, \hat{a}_j^\dagger(t)|0\rangle\, \langle 0|\hat{a}_j(t') \\ &= \frac{1}{\mathcal{N}} \int dt \int dt' G_j^{(1)}(t',t)\, |t\rangle_j\, {}_j\langle t'|, \end{aligned} \tag{43}$$

which in general represents a mixed state, unless the coherence function $G_j^{(1)}(t,t')$ is factorable in its arguments. For equal times, $G_j^{(1)}(t,t) = \langle \hat{a}_j^\dagger(t)\hat{a}_j(t)\rangle = \mathcal{I}_j(t)$ gives the temporal intensity profile of the jth wave, i.e., the probability distribution of detecting the photon at time t at the crystal exit face. The spectral distribution of the heralded photon can be obtained via

$$S_j(\Omega) = \langle \hat{a}_j^\dagger(\Omega)\hat{a}_j(\Omega)\rangle = \int \frac{dt\, dt'}{2\pi} e^{i\Omega(t-t')} G_j^{(1)}(t,t'). \tag{44}$$

Finally, the second-order coherence function in each signal or idler arm can be written as

$$\begin{aligned} G_{jj}^{(2)}(t,t') &= \langle \hat{a}_j^\dagger(t)\hat{a}_j(t)\hat{a}_j^\dagger(t')\hat{a}_j(t')\rangle \\ &= \mathcal{I}_j(t)\delta(t-t') + \mathcal{I}_j(t)\mathcal{I}_j(t') + \left|G_j^{(1)}(t,t')\right|^2 \\ &= \mathcal{I}_j(t)\delta(t-t') + O(g^4). \end{aligned} \tag{45}$$

At leading order in g it describes a delta-correlated Poisson statistics. The corrective terms on the order $O(g^4)$ can be calculated only within a quantum field formalism (see, e.g., [14]), but are exactly zero in the biphoton state formalism (3), in which there are never two photons in the same arm (see the discussion in [14]). As recognized in [34], a measurement of this intensity autocorrelation may provide a direct information on the Schmidt number.

For the sake of brevity, we limit our analysis to the cases of (a) long-pump pulses, where the state is highly entangled, and (b) conditions where nearly separable states can be realized.

A. Long-pump pulses, high entanglement

According to the previous results, when $T_p \gg |\tau_i^\pm| \geqslant |\tau_s|$ the two-photon state is highly entangled in any configuration. We can, for example, use the asymptotic form (37) of the joint temporal amplitude (33), and insert it into formulas (41) and (42). The coherence functions of the signal and the idler obtained in this way are identical (apart from negligible delays), and have the form

$$G_s^{(1)}(t,t') = G_i^{(1)}(t,t') \to \frac{g^2}{2\Delta\tau}\left|\alpha_p(t)\right|^2 \mathrm{Tri}\left(\frac{t'-t}{2\Delta\tau}\right), \tag{46}$$

where $\Delta\tau = |\tau_i^\pm - \tau_s|$, and

$$\mathrm{Tri}\left(\frac{\delta t}{2\Delta\tau}\right) = \begin{cases} 1 - \frac{|\delta t|}{2\Delta\tau}, & \delta t \epsilon (-2\Delta\tau, +2\Delta\tau) \\ 0, & \text{elsewhere} \end{cases} \tag{47}$$

is the triangular function, which has the shape of a triangle of base $4\Delta\tau$ and unitary height. This result is the generalization of formula (46) in Ref. [22]. Actually, it holds for any PDC configuration provided that the bandwidths in play are not too broad because it makes only use of the linear approximations (8) and (11). It shows that when the pump pulse is much longer than the two characteristic time scales, the twin photons have identical properties. The width $\Delta\tau$ of $G^{(1)}(t,t')$ as a function of the time difference $t'-t$ is their *coherence time*, which in this limit is equal to their mutual correlation time [see Eq. (A1)]. Conversely, the temporal distributions of twin photons follow the profile of the much longer pump pulse:

$$\mathcal{I}_s(t) = \mathcal{I}_i(t) = \frac{g^2}{2\Delta\tau}|\alpha_p(t)|^2. \tag{48}$$

Notice that from the point of view of classical statistics of light, this behavior of the $G^{(1)}$, with the peak at $t = t'$ much narrower of the intensity distribution is typical of multimode incoherent light. On the other hand, in the quantum description, the state of the heralded photon in Eq. (43) is in this case mixed because $G_j^{(1)}(t,t')$ in Eq. (46) is not factorable in its arguments.

The spectra of the photons have the usual sinc^2 shape characteristic of spontaneous processes

$$S_s(\Omega) = S_i(\Omega) = \frac{g^2}{\sqrt{4\pi}} T_p \mathrm{sinc}^2(\Omega\Delta\tau), \tag{49}$$

and their spectral bandwidths $\Delta\Omega_j = \frac{1}{\Delta\tau}$ are the inverse of the correlation-coherence times. Clearly, this explains why counterpropagating twin photons are narrow band (order 10 GHz), while copropagating twin photons are in general broadband (order Thz or more)

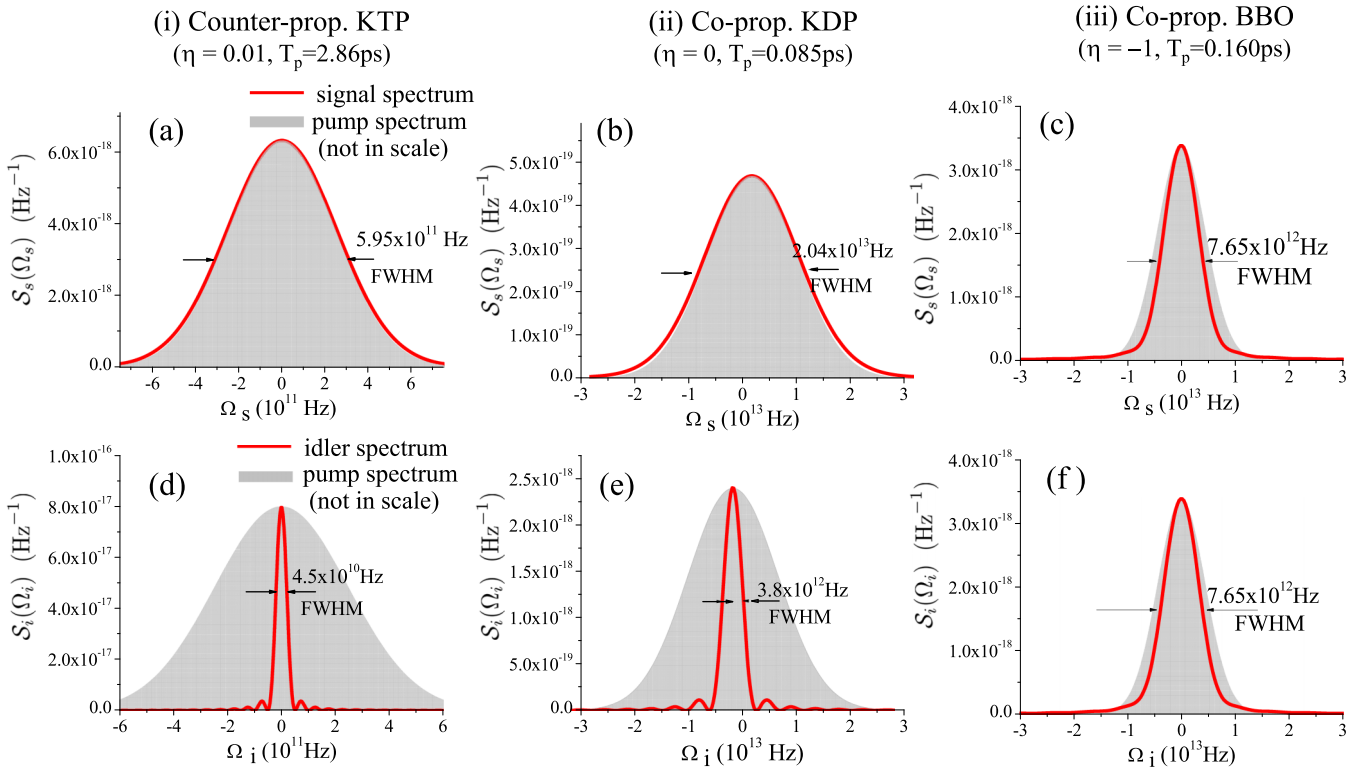

FIG. 6. Spectra of the signal (top) and of the idler (bottom) for the three examples in Table I, in conditions of separability of the state, corresponding to panels (b), (f), and (h) of Figs. 4 and 5. Red lines: signal or idler spectra, numerically calculated. Gray areas: pump spectra. Notice in columns (i) and (ii) the Gaussian profiles of the signal, matching the pump, and the narrower sinc^2 profiles of the idler spectra as predicted by Eqs. (52) and (55).

B. Nearly separable regime

We start from the case $\eta \ll 1$, including both the counterpropagating and the copropagating cases with asymmetric group-velocity matching. We remind that for a pump pulse intermediate between the two time scales $|\tau_i^{\pm}| \gg T_p \gg |\tau_s|$, one photon propagates locked under the pump while the other separates from it after being generated. For this reason, the properties of the two photons are strongly asymmetric as, e.g., shown by the spectra in columns (i) and (ii) of Fig. 6. By using the asymptotic limit (39) of the joint temporal amplitude, and inserting it into formulas (41) and (42), we obtain for the signal photon

$$G_s^{(1)}(\bar{t}_s,\bar{t}'_s) = \frac{g^2}{2\Delta\tau}\alpha_p^*(\bar{t}_s)\alpha_p(\bar{t}'_s), \tag{50}$$

which implies that

$$\mathcal{I}_s(t) = \frac{g^2}{2\Delta\tau}|\alpha_p(t - t_{\mathrm{As}})|^2, \tag{51}$$

$$S_s(\Omega) = \frac{g^2}{2\Delta\tau}|\tilde{\alpha}_p(\Omega)|^2, \tag{52}$$

i.e., the photon that propagates locked under the pump entirely inherits the spectrotemporal properties of the coherent pump laser.

Conversely, for the idler photon

$$G_i^{(1)}(t,t') = \frac{g^2}{2\Delta\tau}\frac{\sqrt{\pi}T_p}{2\Delta\tau}\mathrm{Rect}\left(\frac{\bar{t}_i}{\Delta\tau}\right)\mathrm{Rect}\left(\frac{\bar{t}'_i}{\Delta\tau}\right), \tag{53}$$

and its properties depend on the dispersion properties of the crystal and on its length, through the parameter $\Delta\tau = |\tau_i^{\pm} - \tau_s|$. In particular,

$$\mathcal{I}_i(t) = \frac{g^2}{2\Delta\tau}\frac{\sqrt{\pi}T_p}{2\Delta\tau}\mathrm{Rect}\left(\frac{t - t_{Ai}}{\Delta\tau}\right), \tag{54}$$

$$S_i(\Omega) = \frac{g^2}{\sqrt{4\pi}}T_p\mathrm{sinc}^2(\Omega\Delta\tau). \tag{55}$$

The temporal distribution of the idler photon is a rectangular pulse of duration $2\Delta\tau$ because for such a short pump, the idler photon distribution reflects simply the fact that it can be generated anywhere in the crystal with uniform probability. Remarkably, since $\Delta\tau \simeq |\tau_i^{\pm}| \gg T_p$, the idler wave packet has a longer duration than the pump itself. In particular, in the counterpropagating case, its duration roughly corresponds to the transit time of the pump along the crystal. The idler spectrum retains the same sinc^2 shape as in the long-pump limit, with a bandwidth $\Delta\Omega_i = 1/\Delta\tau \ll \Delta\Omega_p$. Hence, when the state is approximately separable, the heralded idler photon is not only pure, but also more monochromatic than the pump laser that drives the process. However, only in the counterpropagating case this result really means that the generated idler photon is narrow band, as shown by Fig. 6(d), while in the copropagating case it is anyway quite broadband [see Fig. 6(e)] because separability requires ultrabroadband pump pulses. Interestingly, in the counterpropagating case, the strong asymmetry between the twin photons, and the fact that the idler is more narrow band than the pump, reflect the unusual

coherence properties of the classical signal and idler field generated above the MOPO threshold, described in [35,36].

The forms of the coherence functions of the signal and idler, $G^{(1)}(t,t') = \sqrt{\mathcal{I}(t)}\sqrt{\mathcal{I}(t')}$, is typical of single-mode light, which possesses classical temporal coherence: indeed, it means that the average length of a temporal fluctuation (the coherence time) is equal to the duration of the wave packet, implying that the statistics is a sort of frozen in time. In the quantum description the states of the heralded signal and idler photon are pure $\hat{\rho}_j = |\psi_j\rangle\langle\psi_j|$, with

$$|\psi_s\rangle = \frac{1}{(\sqrt{\pi}T_p)^{1/2}} \int dt_s \alpha_p(t_s - t_{A_s})\, \hat{a}_s^\dagger(t_s)|0\rangle, \tag{56}$$

$$|\psi_i\rangle = \frac{1}{\sqrt{2\Delta\tau}} \int dt_i \mathrm{Rect}\left(\frac{t_i - t_{Ai}}{\Delta\tau}\right) \hat{a}_i^\dagger(t_i)|0\rangle. \tag{57}$$

Finally, we consider the alternative technique for reaching separability, i.e.. the configuration with $\tau_s = -\tau_i$ ($\eta = -1$), in which the two photons copropagate symmetrically delayed with respect to the pump center. As can be intuitively understood, in this case the properties of the twin photons are completely symmetric. The mere linear approximation does not give particularly expressive results, so that we have to resort to the stronger Gaussian approximation. According to it, separability is reached at $T_p = T_p^{\min} = \sqrt{2\gamma}|\tau_i^-|$, where (calculations not reported here) the state of each heralded photon becomes pure, $G_j^{(1)}(t,t') = \sqrt{\mathcal{I}_j(t)}\sqrt{\mathcal{I}_j(t')}$, with the temporal and spectral distributions of the two waves given by

$$\mathcal{I}_s(\bar{t}_s) = \mathcal{I}_i(\bar{t}_i) \propto e^{-\frac{(t-t_{Aj})^2}{2T_p^2}} = \left|\alpha_p\left(\frac{\bar{t}_j}{\sqrt{2}}\right)\right|^2, \tag{58}$$

$$S_s(\Omega) = S_i(\Omega) \propto \left|\alpha_p\left(\sqrt{2}\Omega\right)\right|^2, \tag{59}$$

i.e., the two waves have similar properties as the pump, but with a slightly longer duration and a slightly narrower spectrum. As shown by panel (iii) of Fig. 6, these Gaussian results are rather close to the exact ones.

C. Mean number of down-converted pairs efficiency

Another important point in view of applications is the efficiency by which heralded pure photons can be generated by the various strategies. Assuming that the state is approximately separable, the efficiency ultimately depends on the probability that at least a photon pair is generated by a pump pulse crossing the crystal.[1] This can be easily calculated from the state (5) as $\frac{\mathcal{N}}{1+\mathcal{N}} \approx \mathcal{N}$ for $\mathcal{N} \ll 1$, where $\mathcal{N}$ is the mean number of photon pairs per pulse. Within the linear approximation, making, e.g., use of Eq. (33) we obtain

$$\mathcal{N} = \int dt_s \int dt_i |\phi(t_s,t_i)|^2 = g^2 \frac{\sqrt{\pi}T_p}{2\Delta\tau}. \tag{60}$$

This formula is valid for any geometry and any value of T_p, provided that $\Delta\tau \neq 0$. Incidentally, since g^2 is proportional to the pump peak intensity $\mathcal{I}_p$, it implies that the number of down-converted photons is proportional to the energy $E_p = \mathcal{I}_p T_p \sqrt{\pi}$ of the pump pulse.

Notice that in the long-pump regime, where the state is highly multimode, the number of down-converted pairs can be rewritten as

$$\mathcal{N} \simeq \frac{g^2}{2}\mathcal{K} \gg g^2, \tag{61}$$

where we used the asymptotic expression of the Gaussian Schmidt number in Eq. (23), $\mathcal{K}_{\mathrm{Gauss}} = \frac{T_p}{\sqrt{2\gamma}\Delta\tau} \simeq \frac{\sqrt{\pi}T_p}{\Delta\tau}$, since $2\gamma\pi \simeq 1$. Thus, the total number of pairs can be seen as the mean number of pairs per mode $\frac{g^2}{2}$, multiplied by the Schmidt number $\mathcal{K}$. When some strategy is used to decrease the number of modes towards $\mathcal{K} \to 1$, the maximum that can be expected is on the order $\mathcal{N} \simeq \frac{g^2}{2}$. However, different strategies lead to different efficiencies.

According to the Gaussian result (25), the best condition for separability corresponds to $T_p = T_p^{\min} = \sqrt{2\gamma|\tau_s\tau_i^\pm|}$. Substituting into Eq. (60), in these conditions we have

$$\mathcal{N} \to \frac{g^2}{2}\frac{\sqrt{2\pi\gamma|\eta|}}{(1-\eta)} \simeq \begin{cases} \frac{g^2}{4} & \text{for } \eta = -1, \\ \frac{g^2}{2}\sqrt{|\eta|} & \text{for } |\eta| \ll 1. \end{cases} \tag{62}$$

Therefore, the symmetric group-velocity matching leads to a down-conversion efficiency close to its maximum value. Conversely, in the asymmetric case $|\eta| \ll 1$ (counterpropagating or copropagating case with asymmetric group-velocity matching) the efficiency is strongly reduced, $\mathcal{N} \ll \frac{g^2}{2}$. This result is quite natural because in the first case, both photons propagate close to the pump, and the three wave packets remain at least partially superimposed along the entire crystal length. In the latter case, the idler wave packet rapidly separates from the pump because $T_p \ll |\tau_i^\pm|$. Since $g \propto l_c$, it effectively works as if the interaction length were reduced to a shorter length

$$l_c \longrightarrow l_c\sqrt{\frac{T_p}{|\tau_i^\pm|}}. \tag{63}$$

According to these results, one may then wonder whether group-velocity matching is really more efficient with respect to filtering the spectral or temporal modes from a multimode state, where $\mathcal{N} \propto \mathcal{K}$ [Eq. (61)]. Indeed, in this case the maximal efficiency $\mathcal{N} = g^2/2$ could be achieved by some form of "clever" filtering, which manages to project the state onto a single Schmidt mode. Even in the worst case that all the modes have the same weight, at least a fraction $1/\mathcal{K}$ of the total photon number would be transmitted. However, practical considerations, which are outside the scope of this work, may lead to conclude that it is anyway better to directly generate a factorable state.

VI. SUMMARY AND CONCLUSIONS

In this work, we provided a systematic study of the generation of pure heralded single photons through spontaneous PDC, comparing different configurations. We developed a general formalism, where all the properties of the source are condensed in two time scales $\tau_s, \tau_i^\pm$ characteristic of the relative propagation of the three waves inside the medium.

[1] Precisely, the emission rate would depend on both the probability of generating a pair in each pulse and the repetition rate of the laser, but the latter in turn depends on the specific experimental implementation.

On the one side, we derived a simple formula for the Schmidt number of entanglement, that permits to evaluate the degree of purity of the heralded photon via a single parameter. On the other side, the less standard analysis in the temporal domain clarifies the role of the two characteristic time scales, and may permit to understand the mechanism under which the temporal correlation between twin photons can be eliminated. We found that one way of eliminating the correlation relies on creating a strong asymmetry between the velocities of the two down-converted waves relative to the pump wave, so that one photon propagates under the pump pulse while the other, for a pump pulse sufficiently localized inside the crystal, separates from it. In these conditions, the timing provided by the pump pulse may be more precise than that offered by detecting any of the twin photons, and the arrival times of the two photons appear uncorrelated. Such an asymmetry in the relative propagation velocities is naturally present in the counterpropagating geometry because of the natural separation of the GVM and the GVS time scales, but requires particular tuning conditions in the copropagating geometry. Because of this unique feature, pure single photons can be in principle heralded from a counterpropagating pair at any frequency by choosing the required poling period. Moreover, they are naturally narrow band, especially the one propagating opposite to the pump, and separability is achieved for a broad range of pump pulse durations.

Another way of eliminating the correlation requires that the twin photons propagate symmetrically delayed with respect to the pump pulse, and can be implemented only for copropagating photons. Also in this case, the timing information which can be gained from a localized pump can be better than from any of the twins, but the required pump duration is ultrashort, and the generated photons are broadband. Although the purity of heralded photons generated in this way appears somehow lower, symmetric group-velocity matching has the advantage of a higher efficiency of pair production because both twin photons propagate close to the pump. Conversely, the asymmetric group-velocity matching and the counterpropagating geometry are characterized by a low efficiency because purity requires that one photonic wave packet separates from the pump pulse, so that the effective interaction length is reduced.

In conclusion, our systematic study may turn useful for optimizing the existing configurations in view of different applications. For example, when narrow-band single photons are required, the choice should be the counterpropagating configuration, which moreover offers more flexibility since it can be virtually implemented for any wavelength, once the technical challenges for the fabrication of crystals with submicrometer poling periods are overcome. In contrast, twin photons emitted in the common copropagating geometry are naturally broadband and can be generated in a separable state only for very short pulses, under particular tuning conditions. Thus, this is the good choice when broadband photons and or high repetition rates are required. Finally, if efficiency is the main issue, the symmetric group-velocity matching can be the best choice.

We also hope that our general analysis, by providing a deeper and more intuitive understanding of the mechanism through which the temporal correlation of twin photons con be eliminated, may stimulate new strategies of heralded photon generation.

APPENDIX A: INTERPRETATION AND DISCUSSION

In order to understand the results of Secs. III and IV, we resort to the very notion of temporal correlation, which relies on the possibility of predicting the arrival time of one photon by detecting the arrival time of its twin, with a precision better than what would be obtained with an unconditional measurement.

Referring for definiteness to the signal photon (the one that in any case copropagates with the pump), we first wonder what is the uncertainty in its arrival time conditioned to detection of the idler. Then, we will compare it with the uncertainty in its arrival time not conditioned on the detection of the idler.

There are actually two distinct mechanisms by which the exit time of one photon can be ascertained by detecting its twin: one is simply based on their simultaneity, the other relies on the possibility to gain information on the point where down-conversion took place.

The first one prevails for long-pump pulses $T_p \gg |\tau_i^{\pm}| \geqslant |\tau_s|$. In these conditions, the idler and signal wave packets propagate under the pump pulse, and detection of neither photon gives information on the point of the crystal where the pair was generated. Thus, our ability to infer the arrival time of one photon by detection of its twin is limited by the degree to which they arrive simultaneously at their end faces, i.e., by the spread of the distribution of their mutual time delays. This is described by the box function in Eq. (33), characteristic of the spontaneous PDC processes, where a photon pair can be generated at any point along the crystal with uniform probability. Accordingly, the delay between the exits of the twins has a flat distribution in the interval $[-\Delta\tau,+\Delta\tau]$[2] where $\Delta\tau := \frac{l_c}{2}|\frac{1}{v_{gs}} \pm \frac{1}{v_{gi}}|$. Notice that counterpropagating photons (+sign) can be delayed up to their transit time along the sample. Conversely, copropagating twins (−sign) exit from the same face, and appear with a small delay ruled by their GVM, the extreme case being when they propagate exactly at the same velocity, in which case the width of the box function vanishes. According to this mechanism, the exit time of the signal can be deduced from that of the idler as

$$\bar{t}_s = \bar{t}_i \quad \text{within } (\delta t_s)_{\text{cond}} \simeq \Delta\tau = |\tau_i^{\pm} - \tau_s| (T_p \gg |\tau_i^{\pm}|), \tag{A1}$$

where $(\delta t_s)_{\text{cond}}$ indicates the spread of the distribution of the signal arrival time conditioned to detection of the idler, i.e., the *correlation time*.

The second mechanism, described by the factor $\alpha_p(\frac{\bar{t}_s-\eta\bar{t}_i}{1-\eta})$ in Eq. (33), prevails for ultrashort-pump pulses $T_p \ll |\tau_s| \leqslant |\tau_i^{\pm}|$. In this case, both photons separate from the pump during propagation, and detection of any of them provides an indication of the point where the pair was generated. By using a rough picture of photons as wave packets propagating without deformation with their group velocities, one can imagine that

[2]For the original time arguments, $t_s - t_i = \bar{t}_s - \bar{t}_i + (t_{\text{As}} - t_{Ai})$. In the copropagating case, the box function is then shifted to the interval $[0,2\Delta\tau]$ while in the copropagating case the shift is negligible.

if a photon pair were generated at a point z_0, and conversion occurred from a pump photon delayed by δt_p from the center of the pulse, then the idler photon would arrive at its end face at time

$$t_i = \begin{cases} \frac{z_0}{v_{gp}} + \frac{z_0}{v_{gi}} + \delta t_p, & \text{counterprop. case} \\ \frac{z_0}{v_{gp}} + \frac{l_c - z_0}{v_{gi}} + \delta t_p, & \text{coprop. case} \end{cases} \tag{A2}$$

i.e., for the barred time argument $\bar{t}_i = t_i - \frac{1}{2}(\frac{l_c}{v_{gp}} + \frac{l_c}{v_{gi}})$:

$$\bar{t}_i = \left(z_0 - \frac{l_c}{2}\right)\frac{2}{l_c}\tau_i^{\pm} + \delta t_p. \tag{A3}$$

The same argument gives the arrival time of its twin signal photon as

$$\bar{t}_s = \left(z_0 - \frac{l_c}{2}\right)\frac{2}{l_c}\tau_s + \delta t_p, \tag{A4}$$

where in the above formulas δt_p can be considered as a Gaussian stochastic variable with variance $T_p/\sqrt{2}$ because a pump photon can be down-converted at any time along the pump pulse, with a probability proportional to the Gaussian pump intensity. Then, by comparing Eqs (A3) and (A4),

$$\bar{t}_s = \bar{t}_i \frac{\tau_s}{\tau_i^{\pm}} + \delta t_p\left(1 - \frac{\tau_s}{\tau_i^{\pm}}\right) = \eta \bar{t}_i + (1-\eta)\delta t_p. \tag{A5}$$

Thus, according to these arguments, the arrival time of the signal conditioned to detection of the idler is

$$\bar{t}_s = \eta \bar{t}_i \quad \text{within } (\delta t_s)_{\text{cond}} \simeq T_p(1-\eta) \quad (T_p \ll |\tau_s|). \tag{A6}$$

These conditional uncertainties have to be compared with the corresponding unconditional uncertainties, i.e., with the spread of the distribution of the exit times of the signal when the idler is not detected. Also here there are two sources of uncertainty, one is the width T_p of the Gaussian distribution of the pump, because the photon can be down-converted from any portion of the pump pulse, the other one is the point of the crystal where down-conversion took place. Depending on the latter, the delay of the signal photon with respect to the center of the pump pulse ranges in the interval $[0, 2|\tau_s|]$ with uniform probability. Clearly, the first mechanism dominates for $T_p \gg |\tau_s|$, as shown by Eqs. (37) and (39), the second mechanism for $T_p \ll |\tau_s|$ [see Eq. (38)]. A more precise analysis, based on the temporal correlation (33), gives

$$(\delta t_s)_{\text{uncond}} = \sqrt{\frac{T_p^2}{2} + \frac{{\tau_s}^2}{3}} \to \begin{cases} \frac{T_p}{\sqrt{2}}, & T_p \gg |\tau_s| \\ \frac{|\tau_s|}{\sqrt{3}}, & T_p \ll |\tau_s| \end{cases} \tag{A7}$$

where $(\delta t_s)_{\text{uncond}}$ is the variance of the distribution of the arrival times of the signal when the idler is not detected.

Summarizing the results, we have the following situation:

(1) For a long-pump pulse $\boldsymbol{T_p \gg |\tau_i^{\pm}| \geqslant |\tau_s|}$, comparing the unconditional and conditional uncertainties in the arrival time of the signal, in Eqs. (A7) and (A1), we see that for such long pumps $T_p \gg |\tau_i^{\pm}|$, the state is in general highly entangled because[3]

$$\frac{(\delta t_s)_{\text{uncond}}}{(\delta t_s)_{\text{cond}}} \simeq \frac{T_p}{|\tau_i^{\pm} - \tau_s|} = \frac{T_p}{|\tau_i^{\pm}|(1-\eta)} \gg 1. \tag{A8}$$

Heuristically, the above ratio also gives an estimate of the number of entangled modes, well in accordance with the asymptotic behavior of the Schmidt number in Eq. (23) for long-pump pulses.

(2) For an ultrashort-pump pulse $\boldsymbol{T_p \ll |\tau_s| \leqslant |\tau_i^{\pm}|}$, the state is again highly entangled because

$$\frac{(\delta t_s)_{\text{uncond}}}{(\delta t_s)_{\text{cond}}} \simeq \frac{|\tau_s|}{T_p(1-\eta)} = \frac{|\tau_s \tau_i^{+}|}{T_p|\tau_i^{\pm} - \tau_s|} \gg 1 \tag{A9}$$

for $T_p \ll |\tau_s|$. Also in this case, the ratio in Eq. (A9) can be considered an estimate of the number of entangled modes, and indeed reproduces the asymptotic behavior of the Schmidt number in Eq. (24).

Following the above arguments, in particular the results (A8) and (A9), there is no chance that the state becomes separable when $\tau_s \simeq \tau_i^{\pm}$. When the two photons propagate in the same direction at similar velocities, in fact, detection of one photon will always provide an extremely precise information about the arrival time of the other, basically because they exit the crystal almost simultaneously. This is the typical situation that occurs in the copropagating case, in the absence of any velocity-matching strategy, and explains why copropagating photons in general display high temporal entanglement.

Conversely, in the counterpropagating geometry the exit times of the twins lack simultaneity because they follow different paths, and this case is naturally characterized by a strong asymmetry between the twins, in particular, $\tau_i^{+} \gg |\tau_s|$. Because of that, the separable limit (39) can be always realized for intermediate pump durations $\tau_i^{+} \gg T_p \gg |\tau_s|$ which need not be ultrashort because τ_i^{+} is a long time scale. This limit physically corresponds to a situation where the forward signal photon always propagates below the pump pulse, but the pump pulse is short enough that the backward photon rapidly separates from it. In these conditions, the temporal localization of the pump provides an absolute timing information on the exit time of the signal, as precise ($\sim T_p$) as the information that can be gained by detecting the idler $\sim T_p(1-\eta) \approx T_p$, and the exit times of the twins appear uncorrelated. Another way of looking at the situation is that the forward photon is locked to the pump so that it cannot provide any information on the point where down-conversion occurred, and by detecting the signal one does not gain any more precise information on the exit time of the backward idler than by not detecting it.

In the copropagating configuration, the same limit can be reached only by creating a strong asymmetry between the propagation velocities of the two photons relative to the pump $|\tau_s| \ll |\tau_i^{-}|$, which in practice requires that the signal is velocity matched to the pump [5,7,8] as in the example (ii). However, in order that the idler separate from the pump pulse

[3]Notice that $0 < (1-\eta) \leqslant 2$, because of Eq. (28).

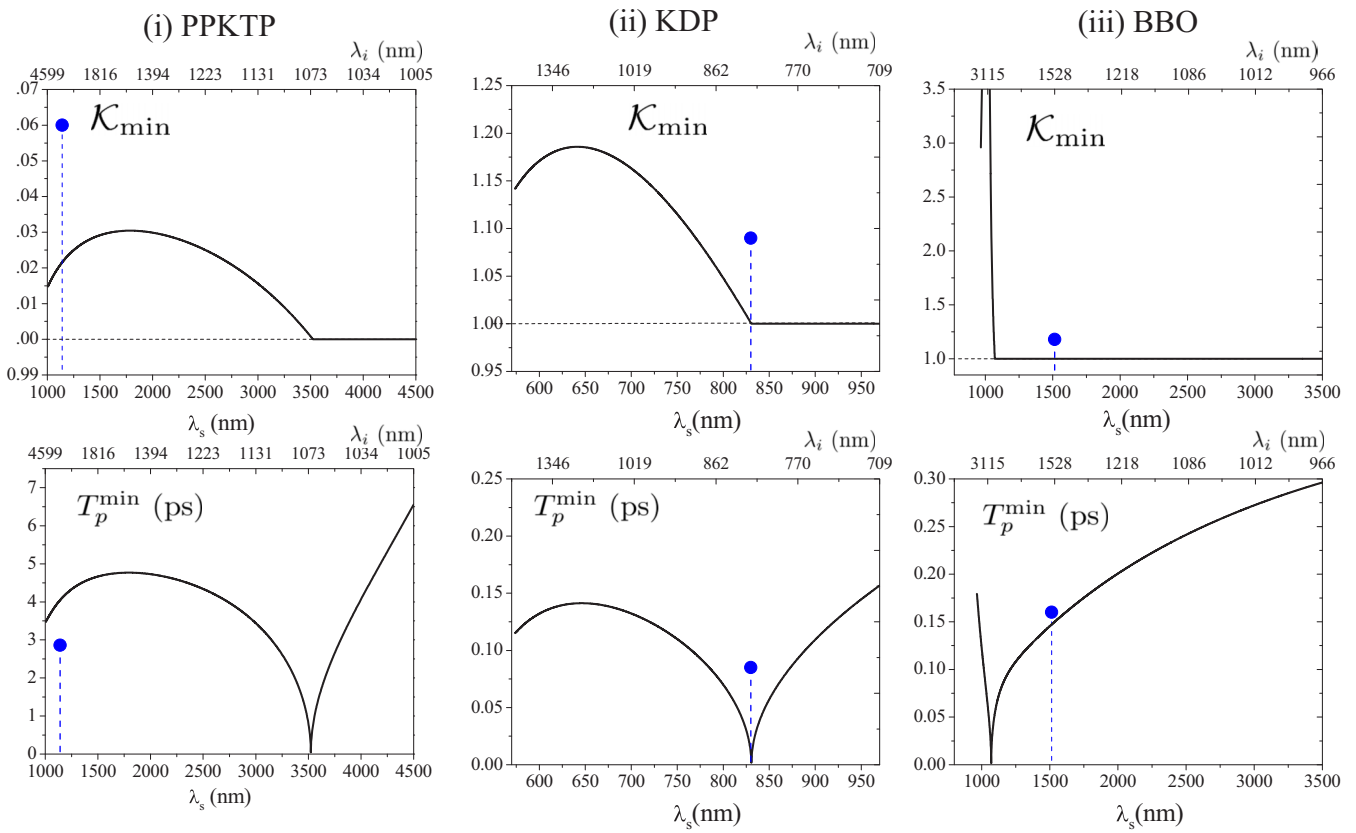

FIG. 7. Comparison between the Gaussian approximation and exact results. Solid lines: minima of the Schmidt number $K_{\min}$ and relative pump durations $T_p^{\min}$ as a function of λ_s, obtained with the Gaussian approximation from Eqs. (26) and (25). Blue dots: exact values calculated at the minima of $\mathcal{K}$ in Fig. 3, numerically evaluated. The top horizontal scale shows the conjugate idler wavelength λ_i.

along a finite propagation length, the pump pulse must be in this case ultrashort [Fig. 4(f)]. As a consequence, the generated twin photons are broadband.

An alternative strategy, which can be realized only in the copropagating case, is the symmetric group-velocity matching [5,13] where twin photons are are symmetrically delayed with respect to the pump center $\tau_s = -\tau_i^-$ and $\eta = -1$, as in the example (iii). Negative values of η are in general favorable to separability because then $\Delta\tau = |\tau_i^{\pm}| + |\tau_s| > |\tau_i^{\pm}|, |\tau_s|$, and twin photons are more simultaneous with the pump than between themselves. In these conditions, a properly localized pump pulse may provide a timing of the exits of the twins more precise than the information that can be inferred from detection of any of them. Focusing on the case $\eta = -1$, when the pump duration T_p approaches $|\tau_i^-| = |\tau_s|$, the twin photons are not enough separated from the pump and cannot provide sufficient information on the point where generation occurred, but on the other side they are no more simultaneous than the pump duration $\Delta\tau = 2|\tau_i^-| > T_p$[4]. As already remarked in Sec. IV, the purity of heralded photons generated in this way is rather far from the ideal result $\mathcal{K}_{\min} = 1$ predicted by the Gaussian formula (26), which seems rather an artifact of replacing the sinc by a Gaussian. The Gaussian approximation (18) has indeed the effect of smoothing the sharp boundaries of the medium at the origin of the sinc function. When taken in the temporal domain it consists in replacing the box function in Eq. (33) by a smooth Gaussian of the same width: $\mathrm{Rect}(\frac{\bar{t}_s - \bar{t}_i}{\Delta\tau}) \to \exp(-\frac{(\bar{t}_s - \bar{t}_i)^2}{4\gamma\Delta\tau^2})$. In this way, the diamond-shaped correlation in Fig. 4(h) becomes a symmetric factorable Gaussian:

$$\phi(\bar{t}_s, \bar{t}_i) \propto \alpha_p\left(\frac{\bar{t}_s + \bar{t}_i}{2}\right)\mathrm{Rect}\left(\frac{\bar{t}_s - \bar{t}_i}{\Delta\tau}\right) \to e^{-\frac{\bar{t}_s^2 + \bar{t}_i^2}{4\gamma(\Delta\tau)^2}} \quad \text{for } T_p = T_p^{\min} = \sqrt{2\gamma}|\tau_i^-|. \tag{A10}$$

APPENDIX B: SPECIFIC CONFIGURATIONS

We considered three configurations suitable for generating pure heralded photons, and a specific example for each configuration:

(i) *Counterpropagating geometry* ($|\eta| \ll 1$). The peculiarity of the counterpropagating geometry is that the condition $|\eta| \ll 1$ is naturally fulfilled, so that any phase-matching configuration has the potentiality to generate pure heralded photons. As a specific example, we considered a 10-mm-long periodically poled crystal of potassium titanyl phosphate (PPKTP) in a type 0 (e-ee) phase-matching configuration: the poling period is $\Lambda = 800$ nm, $\lambda_p = 814.5$ nm, $\lambda_s = 1145$ nm, $\lambda_i = 2932.4$ nm, $\eta = \tau_s/\tau_i^+ = 0.01$. Apart from the length of the crystal, the parameters are those of the experiment reported in [17], and are not particularly optimized for separability. Notice that for the same crystal, the condition $\eta = 0$ can be also realized, and would lead to a higher degree of purity, as discussed in Ref. [14]. For the copropagating geometry, we

considered two examples of asymmetric $\eta = 0$ and symmetric group-velocity matching ($\eta = -1$), taken from the literature [5–8], in particular the example (II) is that of the experiment by Mosley *et al.* [7].

(ii) *Copropagating geometry, asymmetric group-velocity matching* $\eta = 0$. We considered a 10-mm potassium dihydrogen phosphate (KDP) crystal cut for type-II collinear phase-matching (e-oe) at degeneracy. When pumped at 415 nm with a tuning angle $\theta_p = 68.7^\circ$ with the crystal axis, the KDP crystal has the peculiarity of displaying a vanishing GVM between pump and the signal field (i.e., $\tau_s = 0$, $\eta = 0$) and is therefore well suited for the generation a separable two-photon state provided that $T_p \ll \tau_i^- = 0.72$ ps [5,8].

(iii) *Copropagating geometry, symmetric group-velocity matching* $\eta = -1$. The symmetric condition $\eta = -1$ can be fulfilled only in the copropagating configuration, and is rather difficult to meet because it requires that the pump inverse group velocity falls exactly midway between the signal and the idler inverse group velocities

$$\tau_i^- = -\tau_s \longleftrightarrow \frac{1}{2}\left(\frac{1}{v_{gs}} + \frac{1}{v_{gi}}\right) = \frac{1}{v_{gp}}. \tag{B1}$$

Provided this relation is satisfied, the two-photon correlation $\psi(\Omega_s,\Omega_i)$ in the Gaussian approximation displays a circular shape for $T_p = T_p^{\min}$ since $c_{12} = 0$ and $c_{11} = c_{22} = 2\gamma {\tau_s}^2$. For the optimized pump pulse duration, the generated twin photons are thus not only uncorrelated but also indistinguishable.

As a specific example, we considered a 10-mm beta-barium triborate (BBO) crystal both cut for type-II collinear phase matching (e-oe) at degeneracy. When pumped at 757 nm with a pump tuning angle $\theta_p = 28.8^\circ$ the condition $\tau_s = -\tau_i^+ = 0.237$ ps, $\eta = -1$ is realized.

Table I summarizes the parameters for three examples chosen as representative of the configurations (i), (ii), and (iii). Figure 7 plots the results of the Gaussian approximation for $K_{\min}$ and $T_p^{\min}$ [Eqs. (26) and (25)], as a function of the signal central wavelength λ_s, for these three examples. The phase-matched wavelengths λ_s and λ_i and the corresponding characteristic times τ_s and $\tau_i^\pm$ are evaluated using the Sellmeier dispersion formula reported in [31–33]. For the PPKTP crystal, different wavelengths correspond to different poling periods Λ, not reported in the figure. For the KDP and BBO crystals, the signal and idler wavelengths are varied by changing the tuning angle θ_p between the pump direction and the crystal axis (not reported in the figure). Notice that in the BBO case η is always negative for $\lambda_s > 1070$ nm, so that according to the Gaussian approximation (26), in this range the state should be separable. Notice also that for $\lambda_s = 1010$ nm the signal and idler group velocities become equal ($\eta = 1$) and the number of modes predicted by the Gaussian formula (26) diverges. In these conditions, $\mathcal{K}$ becomes indeed very large but not infinite, as it is limited by group-velocity dispersion, a feature not taken into account in the Gaussian model based on linearization (8) and (11).

[4] Quantitatively, when the pump duration approaches $|\tau_i^\pm|$ in Eq. (A8), or $|\tau_s|$ in Eq. (A8), then the ratio $\frac{(\delta t_s)_{\text{uncond}}}{(\delta t_s)_{|\tau_i|}} \to \frac{1}{1+|\eta|} < 1$.

[1] M. D. Eisaman, J. Fan, A. Migdall, and S. V. Polyakov, Rev. Sci. Instrum. **82**, 071101 (2011).

[2] *Single-Photon Generation and Detection: Physics and Applications*, edited by A. Migdall, S. Polyakov, J. Fan, and J. Bienfang, Experimental Methods in the Physical Sciences Vol. 45 (Academic, Waltham, MA, 2013).

[3] A. Christ, A. Fedrizzi, H. Hbel, T. Jennewein, and C. Silberhorn, in *Single-Photon Generation and Detection Physics and Applications*, edited by J. F. Alan Migdall, Sergey V. Polyakov, and J. C. Bienfang, Experimental Methods in the Physical Sciences Vol. 45 (Academic, Waltham, MA, 2013), Chap. 11, pp. 351–410.

[4] A. McMillan, Y.-P. Huang, B. Bell, A. Clark, P. Kumar, and J. Rarity, in *Single-Photon Generation and Detection Physics and Applications*, edited by J. F. Alan Migdall, Sergey V. Polyakov, and J. C. Bienfang, Experimental Methods in the Physical Sciences Vol. 45 (Academic, Waltham, MA, 2013), pp. 411–465.

[5] W. P. Grice, A. B. U'Ren, and I. A. Walmsley, Phys. Rev. A **64**, 063815 (2001).

[6] A. B. U'Ren, C. Silberhorn, K. Banaszek, I. A. Walmsley, R. Erdmann, W. P. Grice, and M. G. Raymer, Laser Phys. **15**, 146161 (2006).

[7] P. J. Mosley, J. S. Lundeen, B. J. Smith, P. Wasylczyk, A. B. U'Ren, C. Silberhorn, and I. A. Walmsley, Phys. Rev. Lett. **100**, 133601 (2008).

[8] P. J. Mosley, J. S. Lundeen, B. J. Smith, and I. A. Walmsley, New J. Phys. **10**, 093011 (2008).

[9] A. L. Migdall, D. Branning, and S. Castelletto, Phys. Rev. A **66**, 053805 (2002).

[10] Z. H. Levine, J. Fan, J. Chen, A. Ling, and A. Migdall, Opt. Express **18**, 3708 (2010).

[11] R. S. Bennink, Phys. Rev. A **81**, 053805 (2010).

[12] A. M. Brańczyk, A. Fedrizzi, T. M. Stace, T. C. Ralph, and A. G. White, Opt. Express **19**, 55 (2011).

[13] L. Zhang, C. Soeller, O. Cohen, B. J. Smith, and I. A. Walmsley, J. Mod. Optics **59**, 1525 (2012).

[14] A. Gatti, T. Corti, and E. Brambilla, Phys. Rev. A **92**, 053809 (2015).

[15] A. Christ, A. Eckstein, P. J. Mosley, and C. Silberhorn, Opt. Express **17**, 3441 (2009).

[16] S. E. Harris, Appl. Phys. Lett. **9**, 114 (1966).

[17] C. Canalias and V. Pasiskevicius, Nat. Photonics **1**, 459 (2007).

[18] C. Canalias, V. Pasiskevicius, R. Clemens, and F. Laurell, Appl. Phys. Lett. **82**, 4233 (2003).

[19] V. Pasiskevicius, G. Strömqvist, F. Laurell, and C. Canalias, Opt. Materials **34**, 513 (2012).

[20] G. Strömqvist, V. Pasiskevicius, C. Canalias, P. Aschieri, A. Picozzi, and C. Montes, J. Opt. Soc. Am. B **29**, 1194 (2012).

[21] T. Suhara and M. Ohno, IEEE J. Quantum Electron. **46**, 1739 (2010).

[22] T. Corti, E. Brambilla, and A. Gatti, Phys. Rev. A **93**, 023837 (2016).

[23] A. Gatti, T. Corti, and E. Brambilla, Phys. Rev. A **96**, 013820 (2017).

[24] A. Gatti and E. Brambilla, Int. J. Quantum Inform. **0**, 1740017 (2017).
[25] J. Monroy-Ruz, K. Garay-Palmett, and A. B. U'Ren, New J. Phys. **18**, 103026 (2016).
[26] T. E. Keller and M. H. Rubin, Phys. Rev. A **56**, 1534 (1997).
[27] A. Ekert and P. L. Knight, Am. J. Phys. **63**, 415 (1995).
[28] S. Parker, S. Bose, and M. B. Plenio, Phys. Rev. A **61**, 032305 (2000).
[29] M. P. van Exter, A. Aiello, S. S. R. Oemrawsingh, G. Nienhuis, and J. P. Woerdman, Phys. Rev. A **74**, 012309 (2006).
[30] A. Gatti, T. Corti, E. Brambilla, and D. B. Horoshko, Phys. Rev. A **86**, 053803 (2012).
[31] G. G. Gurzadian, V. G. Dmitriev, and D. N. Nikogosian, *Handbook of Nonlinear Optical Crystals* (Springer, Berlin, 1991).
[32] K. Kato and E. Takaoka, Appl. Opt. **41**, 5040 (2002).
[33] F. Zernike, J. Opt. Soc. Am. **54**, 1215 (1964).
[34] A. Christ, K. Laiho, A. Eckstein, K. N. Cassemiro, and C. Silberhorn, New J. Phys. **13**, 033027 (2011).
[35] G. Strömqvist, V. Pasiskevicius, C. Canalias, and C. Montes, Phys. Rev. A **84**, 023825 (2011).
[36] C. Montes, B. Gay-Para, M. D. Micheli, and P. Aschieri, J. Opt. Soc. Am. B **31**, 3186 (2014).